Mass Control of Pneumatic Soft Continuum Actuators with Commodity Components

Raphael Deimel Marcel Radke Oliver Brock

***Abstract*— Soft pneumatic hands offer the advantage of intrinsic mechanical compliance. We argue that to fully leverage the compliance available in soft pneumatic actuators, they should be controlled using air mass rather than position or force, as is customary in most research in soft robotics. We propose an air-mass controller that can servo to a preset position and also allows for the exploitation of fast, mechanical compliance without additional control burden. The proposed mass control scheme is based on discrete commodity valves and pressure sensors, filling a gap in available mass control systems for small-scale soft continuum actuators. The proposed mass controller exhibits low drift for mass trajectories lasting tens of seconds, without requiring a precise model of the actuator. Continuous mass control enables applications for soft robotics, in which leveraging compliance during actuation is of central importance.**

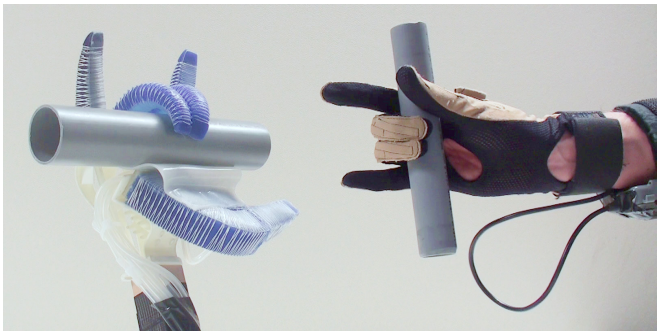

Fig. 1. Example application: Teleoperation of four fingers of an RBO Hand 2 using mass control

I. Introduction

Soft pneumatic hands, such as the RBO Hand 2 (Fig. 1), leverage mechanical compliance to produce robust grasping behavior. Such hands excel in establishing stable contact by compliantly adapting to the shape of the manipulated object. Mechanical compliance achieves this beneficial effect without increasing the requirements on control and sensing.

To fully utilize the advantages of mechanical compliance in soft robotics in general and soft pneumatic hands in particular, their control should focus on putting compliance to work, rather than counteracting it by controlling either position or force, as is customarily done for both "hard" and soft hands [1]–[3]. Consequently, we propose to control the behavior of soft pneumatic hands (and actuators) through *a)* compliance, i.e. a force-position gradient and, at the same time, *b)* preset position, i.e. the position attained when no external forces are applied.

The compliance of most soft pneumatic continuum actuators, such as PneuFlex [4], PneuNet [5], Pneumatic Artificial Muscles, and others [3], [6]–[9] is determined by the structure and material of the actuator, so control cannot change it. The preset position, however, can be changed by inflating and deflating the actuator. The crucial observation is that the natural and straightforward control variable for the preset position is not pressure, but the mass of air enclosed in those actuators. While both can be used to change the preset position, only air mass is independent of the actuator's actual position, which is desirable as it is not determined by the controller, but by the (desired!) compliant interactions with the environment.

Mass control is not a novel concept. However, relevant work on pneumatic control only addresses mass-flow estimation in the context of pressure and position control [10], [11], where accuracy and low drift are not essential. Integrated commercial solutions, such as Festo VPWP valves [12], exist but their nominal flow rates (350 to 1400 slpm, standard liters per minute) are two to three orders of magnitude higher than what is required for the typical soft hand. We can therefore conclude that existing commercial solutions to mass control are not suitable for a broad range of applications in soft robotics, where masses and flow rates are relatively small and drift plays a significant role.

In this paper we present a simple yet effective method for mass control, with flow rates adaptable from 100 slpm down to 0.1 slpm. This range is suitable for the control of soft robotic hands and many other pneumatic systems in soft robotics. The control method operates on discrete valves and pressure sensors. Both components are used much more frequently [3], [6], [7], [13] than expensive mass-flow sensors or proportional control valves.

While discrete valves are attractive from the perspective of size and cost, two main problems arise in the context of mass control. Without additional sensors on the actuator, mass can only be estimated via integrating the mass-flow at the valve, making it subject to drift. The second problem arises from using discrete valves, which cannot create infinitely short pulses, resulting in hysteresis. In our approach, drift is minimized by learning a model to accurately predict change of mass from pressure sensor and valve actuation state in Section III, while hysteresis is minimized by the choice of hardware, as explained in IV.

All authors are with the Robotics and Biology Laboratory, Technische Universität Berlin, Germany.

We thank Ivo Boblan for valuable input on pneumatic control strategies.

We gratefully acknowledge financial support by the European Commission (SOMA, H2020-ICT-645599) and by the Alexander von Humboldt foundation and the Federal Ministry of Education and Research (BMBF).

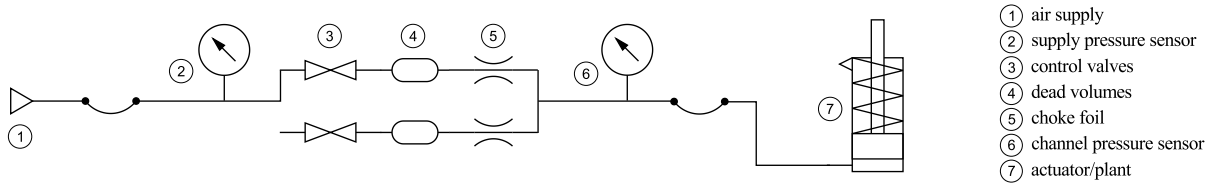

Fig. 2. Schematic control path of the pneumatic control system using discrete valves and pressure sensors

Our experiments demonstrate the feasibility of accurately controlling soft hands via mass based on discrete valves. The proposed controller has low drift, enabling the fast and stable tracking of smooth preset position trajectories tens of seconds in duration. This capability closes a gap in soft hand control and opens up applications where compliant and synchronized motion plays a central role.

II. Related work

Most pneumatic control systems are designed for position or force control [1]–[3], [8], [14]. For both, pressure is the most natural choice of control variable. However, we want to control the preset position via mass. As a result, this precludes the use of commercially available servo pneumatic systems, which usually provide position control. For control of the preset position, actuator pressure is not a suitable control variable as it varies through contact of the environment — the normal situation when we want to leverage the compliance of soft actuators.

For the type of soft continuum actuator we use in this paper, two control methods are described in literature, both based on position control by pressure. A recent attempt to create smooth, continuous actuator control was published by Polygerinos et al. [2]. Marchese and Rus [1] developed a comprehensive position control system for soft continuum actuators which requires electromechanically actuated cylinders to control pressure.

The controller for the pneumatically driven Shadow hand [15] decomposes control into position and compliance, whereas we decompose control into preset position and compliance. While the former controller treats the position of the actuator as the key control variable, our approach leaves the position free so as to exploit compliance. We believe this is advantageous when the exploitation of compliance is required by the application.

Carneiro and de Almeida [11] perform position control, where they employ an artificial neural network to linearize mass flow of servo valves w.r.t. their command input. If a control system is based on proportional valves, this approach could also be used for mass control, even though the authors do not implement this. In contrast, the approach presented here relies on discrete valves which are more widely in use.

Control of mass has generally been neglected in favor of controlling pressure. This is surprising, as mass provides a meaningful proxy of actuator state, which is particularly relevant for soft continuum actuators. In this paper we attempt to close this gap by presenting a simple to implement, high-performance mass controller.

III. Mass Control Model

We want to design a controller for the pneumatic system illustrated in Fig. 2. Two sensors provide measurements of the supply pressure and the pressure directly after the valve, while ambient pressure is assumed to be known and constant. These sensors are used to estimate the air mass passing through the valve during an opening cycle (we will refer to this as a *pulse*). The controller opens a valve when the error between currently estimated and desired mass exceeds a threshold. Once the valve is open, the controller continuously monitors the estimate and closes the valve when the error changes sign.

The controller obtains a mass estimate through the integration of mass flow. Consequently, control is subject to drift as estimation errors accumulate. It is therefore paramount for reliable control to estimate mass flow as accurately as possible across many different pulse lengths and pressure ranges. To achieve this, we model the flow path with a linear combination of well known effects from fluid dynamics [16] plus effects caused by switching delays:

$$\begin{aligned} m(\Delta t) = \quad & c_0 && \text{Bias} \\ & + c_1 \cdot \int_{t_{on}}^{t_{on}+\Delta t} (p_{in}(t) - p_{out}(t))dt && \text{Friction} \\ & + c_2 \cdot \int_{t_{on}}^{t_{on}+\Delta t} p_{in}(t) \cdot \Psi(t)dt && \text{Injector} \\ & + c_3 \cdot p_{in}(t_{on}) + c_4 \cdot p_{out}(t_{on}) && \text{Switching} \end{aligned} \tag{1}$$

where p_{in} and p_{out} denote absolute inlet and outlet pressure and Δt the duration of the pulse. The *bias* term models sensor bias, *friction* models viscous friction along the inner walls of the flow path, *injector* models choke behavior, and *switching* models effects by the dead volume and valve timing. As the flow path volume used for estimation is small, we do not need to model inertial and temperature effects. The parameters $c_0, \ldots, c_4$ are determined via linear regression as explained in Sec. V. The function $\Psi(t) = \Psi(p_{in}(t), p_{out}(t))$ captures the non-linearity of a choke or valve and is well known in fluid dynamics [16].

To simplify computation of the injector term, we use an approximation (Eq. 2) published by The Lee Company [17]:

$$\begin{aligned} \psi &\approx \sqrt{\frac{p_{in} - p_{out}}{p_{in}} \cdot \frac{p_{out}}{p_{in}}} && \frac{p_{in}}{p_{out}} < 1.894 \\ \psi &\approx 0.5 && \frac{p_{in}}{p_{out}} > 1.894 \end{aligned} \tag{2}$$

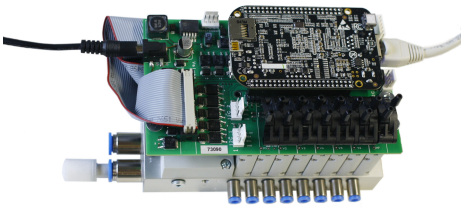

Fig. 3. The control system consists of a single-board-computer, input/output PCB, valve array and pressure sensors.

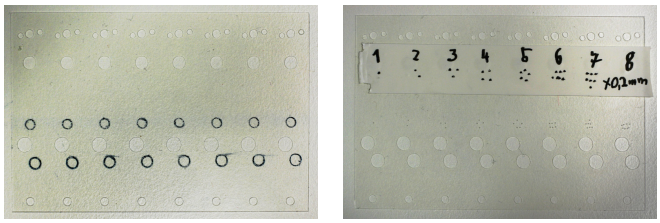

Fig. 4. A PET foil is placed under the valves on the socket to reduce nominal flow. Left: Pre-cut template with areas marked to be pierced. Right: Configured foil with a number of $0.2\,\mathrm{mm}$ holes at the inlet and $4\,\mathrm{mm}$ holes at the outlet path.

The top and bottom terms model subsonic flow and sonic flow respectively. The approximation results in an acceptably low increase in root-mean-square-error (RMSE) of 1.4% in the evaluation experiments.

The mass is estimated continuously during inflation and deflation and is used for bang-bang control of the mass. The minimal attainable mass change is determined by the valve's switching delays and the dead volume between valve and choke. It is discussed in detail in Section IV.

IV. Controller Hardware

The mass control model described in the previous section is based on discrete valves, requires pressure sensors, and is implemented on a real-time control unit. All components are shown in Fig. 3. We use a valve array with eight standard 5/3 pilot valves (Festo VTUG series), each providing three states for inflation, deflation, and for disconnecting the plant. The switching times of the valves range from $20\,\mathrm{ms}$ to $40\,\mathrm{ms}$. Actuator pressure is measured with a Freescale MPX4250 ($250\,\mathrm{kPa}$ range, 1.4% accuracy), supply pressure with a MPX5700 ($700\,\mathrm{kPa}$ range, 2.5% accuracy). The real-time control unit is a single board computer (BeagleBone Black). The controller runs at $500\,\mathrm{Hz}$. Valves, sensors, and control unit are connected with a custom adapter PCB.

To allow fine-grained mass control, we reduce the smallest attainable change of air mass in two ways. First, the valve is choked to reduce air flow, which reduces the amount of air flowing during the minimum opening period of the valve used. Second, we place the choke as close as possible to the valve to minimize the length of the flow path in between. This is important, as the volume along that section (the dead volume indicated as (4) in Fig. 2) is pressurized (or depressurized) almost instantly when the valve opens, increasing hysteresis.

Choking is realized by placing a $0.1\,\mathrm{mm}$ thick PET foil (Fig. 4) between the valves and their aluminum array socket. This placement minimizes the dead volume to $0.15\,\mathrm{cm}^3$. The foil is prepared using a cutting plotter (Silhouette Portrait). The inlet and outlet holes are pierced afterwards, using needles of different sizes. This allows us to adjust the nominal air flow by two orders of magnitude. In our experiments, the foil has a $0.2\,\mathrm{mm}$ hole along the inflation path and a $0.6\,\mathrm{mm}$ hole along the deflation path to balance inflation and deflation speed.

V. Calibration

As the exact structure and behavior of the control hardware is usually not known, an important aspect of the mass-controller is calibration of the mass observer model. We devised a mostly automated calibration procedure which only requires user interaction to vary supply pressure (Algorithm 1). We attach a known, fixed volume to the channel and gather data from a predefined range of channel pressures (p_{min}, p_{max}), pulse durations (t_{min}, t_{max}) and supply pressures (manual). Channel pressure is swept gradually by skewing the ratio of inflation to deflation period. The change of mass is estimated via the ideal gas law and the change of channel pressure. Eq. 1 coefficients are computed separately for inflation and deflation pulses, as air passes through different flow paths.

Algorithm 1 Calibration procedure

skew factor $\leftarrow 2.0$
$n_{\text{supply}} \leftarrow \frac{n_{\text{samples}}}{5}$
$skew \leftarrow \sqrt{\text{skew factor}}$
for i in $[1 \ldots n_{\text{samples}}]$ **do**
  if $p_{channel} < p_{min}$ **then** $skew \leftarrow \sqrt{\text{skew factor}}$
  else if $p_{channel} > p_{max}$ **then** $skew \leftarrow \sqrt{\frac{1}{\text{skew factor}}}$
  end if
  if $i \mod n_{\text{supply}} = 0$ **then**
    Request variation of supply pressure
  end if
  $t \leftarrow$ RandomExponential($t_{min}, t_{max}, \lambda = 1$)
  $t_{inflation} \leftarrow t \cdot skew$
  $t_{deflation} \leftarrow t \cdot \frac{1}{skew} \cdot \frac{\text{deflation speed}}{\text{inflation speed}}$
  Record $p_{channel}, p_{supply}$
  Inflate($t_{inflation}$)
  Record $\Delta p_{channel}$ and Eq. 1 terms
  Compute ground truth Δm from $\Delta p_{channel}$
  Record $p_{channel}, p_{supply}$
  Deflate($t_{deflation}$)
  Record $\Delta p_{channel}$ and Eq. 1 terms
  Compute ground truth Δm from $\Delta p_{channel}$
end for
Compute $c_0 \ldots c_4$ on inflation data points using linear regression
Compute $c_0 \ldots c_4$ on deflation data points using linear regression

For a typical channel calibration, 200 individual data points are recorded for each flow path. A settling period of $1\,\mathrm{s}$ before reading pressures guards against residual airflow. The term $\frac{\text{deflation speed}}{\text{inflation speed}}$ is a rough estimate to approximately balance the duration of upwards and downwards sweeps. Due to the exponential distribution of t, linear regression is biased

towards better fitting shorter pulses. This is intentional as short pulses usually occur more often than long ones.

VI. Mass Control Performance

Two important aspects are evaluated in this section: the attainable improvement in accuracy over using precomputed inflation periods and the drift of mass. Ground truth for this evaluation was acquired by computing the contained air mass post-hoc by applying the ideal gas law $m = \frac{p \cdot V}{R \cdot T}$ on a fixed, constant volume. Pressure was measured before and after inflation.

Evaluation of the mass observer was done by gathering data on ten different inflation and deflation pulses lasting $40\,\mathrm{ms}$ to $1000\,\mathrm{ms}$, starting from five different initial pressure values, and executed with four different supply pressures from $260\,\mathrm{kPa}$ to $350\,\mathrm{kPa}$ to obtain a total of 200 data points. The individual terms of Eq. 1 were computed individually at $500\,\mathrm{Hz}$.

We compare the proposed mass observer with a control that was used in previous work [4], [13]:

$$m(\Delta t) = c_0 \cdot \Delta t \cdot p_{in}(t_{on}) \tag{3}$$

The model assumes mass flow to be constant during inflation and to only depend on the presumably constant inlet pressure. These assumptions make it possible to precompute the required pulse duration.

A. Overall Improvement to Accuracy

Fig. 5 shows the overall improvement in mass estimation when using a calibrated mass-flow estimator (Eq. 1) relative to the naive model (Eq. 3). The former reduces absolute error by approximately a factor of five. Errors are computed with respect to ground truth.

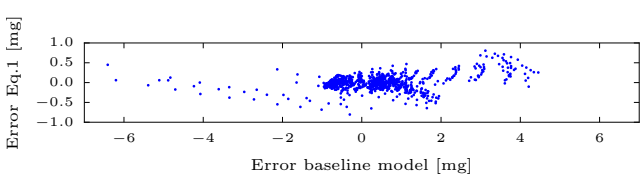

Fig. 5. Change of error when switching from the baseline model (x-axis) to a model employing Eq. 1 (y-axis)

Fig. 6 visualizes the performance of both models against ground truth. At inflation (positive mass change), both the baseline model and the full model perform equally well. This can be explained by the large pressure drop at the choke, which puts the model into the sonic region where airflow is only determined by inlet pressure. At deflation though, the full model exhibits superior accuracy.

B. Contribution of individual model terms

We evaluate the individual contribution of the model's terms to the root-mean-square-error (RMSE) of the mass estimate. Errors of selected subsets are given in Table I. The full model (Eq. 1) improves accuracy over the baseline by a factor of seven. The biggest improvement can be obtained by

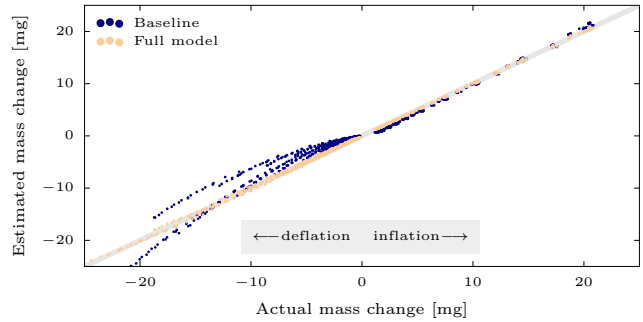

Fig. 6. Performance of the full model compared to the baseline model.

Baseline	1.325 mg
Full model	0.179 mg
Model w/o Injector	0.804 mg
Model w/o Bias and Switching	0.431 mg
Model w/o Bias	0.182 mg
Model w/o Switching	0.188 mg
Model w/o Friction	0.188 mg

TABLE I

RMSE of mass observer variants and the baseline model.

including the *injector* term, followed by either the *switching* term or a constant *bias*. Removing only either *switching* or *bias* does not change RMSE much, which indicates a large overlap between both terms. When excluding the *friction* term, RMSE increases only by 5.0%, which indicates that viscous friction does not play a significant role in our setup. Nevertheless, it may be advisable to keep this term for other setups, e.g. miniature solenoid valves which have narrower flow paths.

Overall, the data presented in this section indicate a considerable improvement over the baseline model. We identified the injector term to be the most important model component, followed by the *switching* term for effects not related to the inflation period.

C. Accuracy

To gauge the variance in attainable accuracy, we calibrated five individual valves and computed the mass error resulting from the sinusoidal test pattern shown in Fig. 7. The training set was reduced to 100 data points by only recording at $260\,\mathrm{kPa}$ and $320\,\mathrm{kPa}$ supply pressure to speed up calibration.

The resulting error is shown in Fig. 8. For all but one valve the error after $60\,\mathrm{s}$ stays below the hysteresis of the hardware.

The mass controller also rejects influence of supply pressure variations. Fig. 9 shows a test run in which the supply pressure varied in a range typical for unregulated compressors. The controller fares well in rejecting the variation, demonstrating that soft hands can potentially be operated with a small on-board compressor in mobile robots without sacrificing performance.

The left plot in Fig. 8 shows the tracking error during a test pattern after calibration. It shows a continuous, systematic buildup of error (drift), which indicates that the model

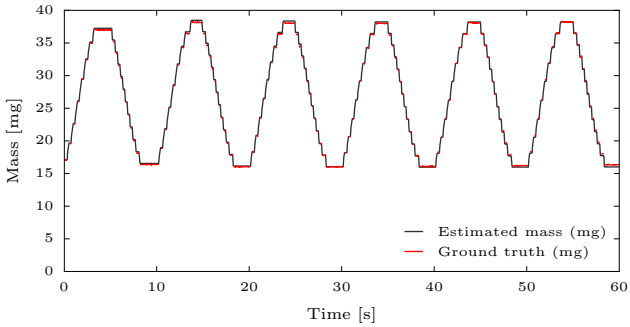

Fig. 7. Tracking performance of one calibrated channel over 60 s and 122 individual pulses

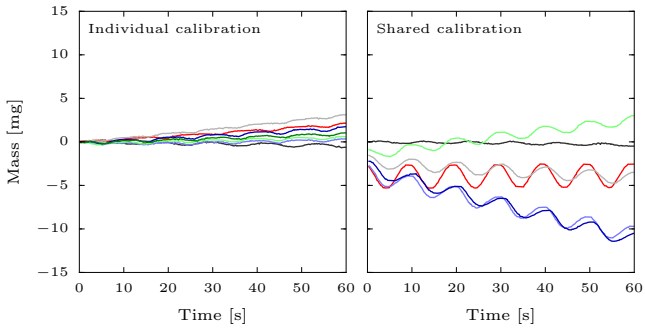

Fig. 8. Tracking error of six individual channels using the sine pattern shown in Fig 7: Performance when calibrating each channel individually (left), performance when sharing a single calibration across identically configured channels (right)

under-fits the actual system behavior. It may therefore be worthwhile to investigate the application of more versatile function approximators (e.g. neural networks [11] or kernel ridge regression) for the observer model.

D. Variability Across Valves

We also evaluated whether valve calibration is required for each individual valve, or if calibration data can be shared for identical configurations, which would greatly simplify calibration. The right plot in Fig. 8 shows the performance when sharing a single calibration. Compared to the same test with individually calibrated valves on the left, the error is almost five times larger. Given this result, every channel should be calibrated individually.

VII. Application

The mass controller enables us to enact mass trajectories on soft hands, but also to adjust actuator state incrementally. These capabilities are tested with the RBO Hand 2 [13] in two applications. In the first application—a benchmarking test—four fingers of the hand are closed and opened in a sinusoidal motion six times. The total duration of the motion is 60 s. This benchmark enables us to assess the amount of drift. In the second application, a human controls the finger posture of the soft hand via a dataglove in a manipulation scenario. This allows us to assess whether control is smooth and reactive enough for teleoperation experiments in grasping. In both tests we attached index,

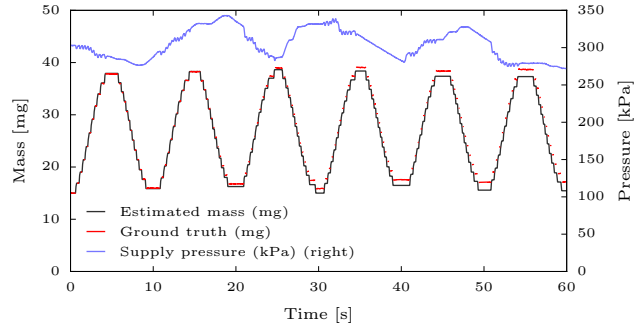

Fig. 9. Changes in supply pressure are automatically compensated by the mass controller, a feature important for mobile applications.

middle, ring, and little finger to four channels, making each controllable independently. Together with the volume added by tubes we require ca. 45 mg of air to bend the fingertip by 180°. The controller's threshold was set to 1.7 mg, which translates to about 7° in fingertip orientation.

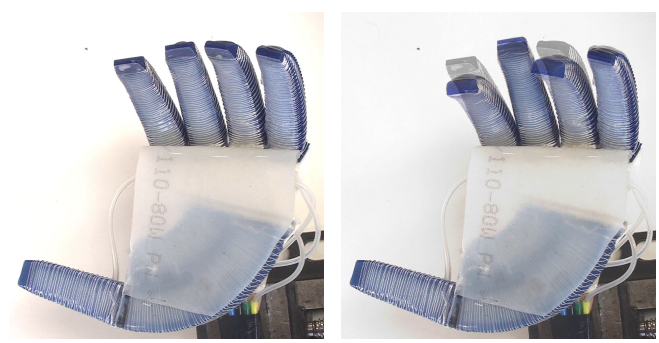

Fig. 10. Effect of drift after sinusoidal finger motion (shown in the video attachment): Initial posture (left), posture after 60 s of continuous motion (right); middle and small finger return to the initial posture, while index and ring finger show a slight deviation.

1) Sinusoidal Finger Motion: The desired mass trajectory was set to a sine wave (10 mg to 40 mg amplitude and 10 s period) for 60 s, starting at 10 mg. Fig. 10 shows the fingertip positions before and after the benchmark. After the entire motion, index and ring finger are slightly more bent by about 10° while the other two finger did not drift at all. Overall, the drift in hand posture is small enough to make the implementation of grasping motions and short in-hand manipulation tasks feasible.

2) Teleoperated Hand: In the second application, the RBO Hand 2 is teleoperated by a human with visual feedback, as shown in Fig. 1. Such a setup enables research on how humans compensate for end effector impairments, but also allows to transfer human manipulation expertise onto robots [18].

To control the RBO Hand 2, the operator wears a dataglove (Cyberglove II). The measurements of PIP and DIP joints are mapped linearly to the desired mass of the corresponding fingers. Posture is only set once at the beginning of interaction, making the setup subject to drift. The human operator is capable of enacting postures, but is also capable to grasp objects and modify the grasps. The drift is sufficiently low

to enable elaborate interactions before resetting the mass estimate becomes necessary. The control hysteresis attained by our hardware is low enough to not negatively affect the interaction with the object.

VIII. Limitations

1) Drift: Mass control based on mass flow integration inherently drifts over time. Therefore, this type of control is best suited for short or moderately long actuation patterns that require less than 20 to 50 pulses. If longer sequences are desired, either additional sensors have to be employed for sensor fusion, or ground truth is acquired at intermediate, well defined hand postures which results in a known channel volume, thereby enabling the computation of mass based on pressure.

2) Leakage: Leakage potentially leads to a mismatch of estimated and actual mass flow. In our experience, all components are sufficiently airtight for this not to be a problem, quick-connect plugs are most prone to introduce noticeable leakage.

3) Hysteresis: The applications presented in Section VII reveal a considerable positioning hysteresis, albeit the actuator's compliance exaggerates the effect. The hysteresis is determined by the product of two factors, the smallest attainable opening period of the valve used and the maximum actuation speed required by the application. The pilot valves used in this paper have a minimum pulse duration of $20\,\mathrm{ms}$ to $40\,\mathrm{ms}$. By adopting solenoid valves, it can be reduced to $1\,\mathrm{ms}$ to $4\,\mathrm{ms}$, providing a tenfold reduction in hysteresis, or alternatively a tenfold increase in actuation speed. Performance can further be improved by pairing two discrete valves, one configured for fast inflation and large hysteresis and one configured for slow inflation and small hysteresis.

IX. Conclusion

We presented a simple yet effective method for mass control of soft continuum actuators and soft hands. The use of mass control (rather than position or force control) is motivated by the importance of compliance for many applications in soft robotics. If the exploitation of mechanical compliance is the target behavior, the control goal for a soft actuator becomes its preset position, i.e. the position attained when no external forces are applied. This preset position is most naturally controlled with air mass, as this does not require control action during the use of compliance in interaction. In contrast, position and force control would require continuous adjustments during the exploitation of mechanical compliance. Mass flow can also be switched on and off almost instantly, enabling high control bandwidth. This stands in contrast to pressure control, where complex flow dynamics reduce control bandwidth and stability depends on the attached plant. Mass, on the other hand, can be estimated without knowledge of the properties of the attached robotic device.

The proposed controller and the demonstrated hardware close a gap in control in soft robotics: Based on low-cost commodity hardware, it is now possible to perform accurate, low-drift mass control. We successfully applied the proposed mass controller to a benchmark problem with a soft actuator and to the teleoperation of a soft hand.

References

[1] A. D. Marchese and D. Rus, "Design, kinematics, and control of a soft spatial fluidic elastomer manipulator," *The International Journal of Robotics Research*, vol. 35, no. 7, pp. 840–869, 2016.

[2] P. Polygerinos, Z. Wang, J. Overvelde, K. Galloway, R. Wood, K. Bertoldi, and C. Walsh, "Modeling of soft fiber-reinforced bending actuators," *Robotics, IEEE Transactions on*, vol. 31, no. 3, pp. 778–789, June 2015.

[3] D. P. Holland, E. J. Park, P. Polygerinos, G. J. Bennett, and C. J. Walsh, "The soft robotics toolkit: Shared resources for research and design," *Soft Robotics*, vol. 1, pp. 224–230, 2014.

[4] R. Deimel and O. Brock, "A compliant hand based on a novel pneumatic actuator," in *IEEE International Conference on Robotics and Automation (ICRA)*, 2013, pp. 2047–2053.

[5] F. Ilievski, A. Mazzeo, R. F. Shepherd, X. Chen, and G. M. Whitesides, "Soft robotics for chemists," *Angewandte Chemie International Edition*, vol. 50, no. 8, pp. 1890–1895, 2011.

[6] B. Mosadegh, P. Polygerinos, C. Keplinger, S. Wennstedt, R. F. Shepherd, U. Gupta, J. Shim, K. Bertoldi, C. Walsh, and G. M. Whitesides, "Pneumatic networks for soft robotics that actuate rapidly," *Advanced Functional Materials*, vol. 24, no. 15, pp. 2163–2170, 2014.

[7] A. Marchese, K. Komorowski, C. Onal, and D. Rus, "Design and control of a soft and continuously deformable 2d robotic manipulation system," in *IEEE International Conference on Robotics and Automation (ICRA)*, May 2014, pp. 2189–2196.

[8] T. Noritsugu, H. Yamamoto, D. Sasakil, and M. Takaiwa, "Wearable power assist device for hand grasping using pneumatic artificial rubber muscle," in *SICE 2004 Annual Conference*, vol. 1, 2004, pp. 420–425.

[9] J. Bishop-Moser, G. Krishnan, C. Kim, and S. Kota, "Design of soft robotic actuators using fluid-filled fiber-reinforced elastomeric enclosures in parallel combinations," in *IEEE/RSJ International Conference on Intelligent Robots and Systems (IROS)*, 2012, pp. 4264–4269.

[10] P. Rapp, M. Weickgenannt, C. Tarín, and O. Sawodny, "Valve flow rate identification and robust force control for a pneumatic actuator used in a flight simulator," in *American Control Conference (ACC)*, 2012, pp. 1806–1813.

[11] J. F. Carneiro and F. G. de Almeida, "Pneumatic servo valve models based on artificial neural networks," *Proceedings of the Institution of Mechanical Engineers, Part I: Journal of Systems and Control Engineering*, vol. 225, no. 3, pp. 393–411, 2011.

[12] Festo AG, "Proportional directional control valves vpwp," https://www.festo.com/cat/en_en/data/doc_engb/PDF/EN/VPWP_EN.PDF, 2016, [Online; accessed 20-Feb-2016].

[13] R. Deimel and O. Brock, "A novel type of compliant and underactuated robotic hand for dexterous grasping," *The International Journal of Robotics Research*, vol. 35, no. 1–3, pp. 161–185, March 2016.

[14] X. Brun, M. Belgharbi, S. Sesmat, D. Thomasset, and S. Scavarda, "Control of an electropneumatic actuator: comparison between some linear and non-linear control laws," *Proceedings of the Institution of Mechanical Engineers, Part I: Journal of Systems and Control Engineering*, vol. 213, no. 5, pp. 387–406, 1999.

[15] F. Rothling, R. Haschke, J. J. Steil, and H. Ritter, "Platform portable anthropomorphic grasping with the bielefeld 20-dof shadow and 9-dof tum hand," in *IEEE/RSJ International Conference on Intelligent Robots and Systems (IROS)*, 2007, pp. 2951–2956.

[16] E. Pilz and E. Becker, *Technische Strömungslehre: Eine Einführung in die Grundlagen und technischen Anwendungen der Strömungsmechanik*. Teubner Studienbücher Mechanik, 1993.

[17] The Lee Company, "How to calculate flow resistance for gases," http://www.theleeco.com/engineering/gases/calculate-flow-resistance-gases.cfm, 2016, [Online; accessed 20-Feb-2016].

[18] C. Eppner, R. Deimel, J. Alvarez-Ruiz, M. Maertens, and O. Brock, "Exploitation of environmental constraints in human and robotic grasping," *The International Journal of Robotics Research*, vol. 34, no. 7, pp. 1021–1038, June 2015.